MATERIALS CHEMISTRY
FRONTIERS

RESEARCH ARTICLE

View Article Online
View Journal | View Issue

Cite this: *Mater. Chem. Front.*, 2017, **1**, 152

Thiophene-derived polymer dots for imaging endocytic compartments in live cells and broad-spectrum bacterial killing†

Kenath Priyanka Prasad,[a] Aung Than,[a] Nan Li,[a] Mahasin Alam SK,[a] Hongwei Duan,[a] Kanyi Pu,[a] Xinting Zheng[b] and Peng Chen*[a]

Received 25th May 2016,
Accepted 29th June 2016

DOI: 10.1039/c6qm00065g

rsc.li/frontiers-materials

In this work, we present a new type of polymer dot synthesized from bithiophene (pTh-Pdot) *via* a simple and high yield procedure. Owing to their high brightness, excellent photo-stability, good biocompatibility, and molecular size, pTh-Pdots are promising for bioimaging applications. As a proof-of-concept demonstration, pTh-Pdots are herein employed to track the endocytic pathway in live cells. Furthermore, we show that these polymeric nanoparticles can serve as potent antibacterial agents by making use of their ability to disrupt bacterial membranes and high peroxidase mimicking activity.

Introduction

In recent years, fluorescent quantum dots or nanoparticles derived from semiconducting polymers (Pdots) have attracted considerable interest for various biomedical applications (*e.g.*, fluorescence and photoacoustic cellular imaging, optical sensing, and photodynamic therapy), owing to their unique properties such as high brightness, tunable and non-blinking emission, broad absorption, high photo-stability, biocompatibility, and molecular size.[1–6] Pdots are usually made by collapsing and packing long-chain fluorescent polymers using, *e.g.*, miniemulsion or reprecipitation methods.[7–9] These Pdots are often large in size and require a tedious synthesis process.

Recently, we synthesized a new type of crystalline Pdot by ultrasonic breakdown of electrochemically polymerized non-fluorescent poly(3,4-ethylenedioxythiophene).[10] Using a similar strategy, we herein fabricate novel Pdots from polythiophene, a semiconducting polymer. These readily synthesized Pdots are of molecular size, bright, and biocompatible. Interestingly, such polythiophene-based Pdots (pTh-Pdots) exhibit negative solvatochromism, *i.e.*, a blue shift in photoluminescence (PL) emission with an increase in solvent polarity. We demonstrate that, likely due to its negative solvatochromism properties, pTh-Pdots fluoresce blue in early endosomes but green in lysosomes, hence allowing tracking of the endocytic pathway in live cells. In addition to their potential for cellular imaging, we further show the use of pTh-Pdots as an excellent antibacterial agent against both Gram-positive and Gram-negative bacteria.

Experimental section

Preparation of polythiophene (pTh) films

The 2,2′-bithiophene (BTh) monomer and ionic liquids (1-*n*-butyl-3-methylimidazolium tetrafluoroborate – $BMIMBF_4$; 1-butyl-3-methylimidazolium methyl sulphate – $BMIMMeSO_4$) were purchased from Sigma Aldrich.

Using a 0.1 M BTh monomer in the ionic liquid $BMIMBF_4$, the poly(2,2-bithiophene) (pTh) film was electro-polymerized onto an ITO working electrode held at the constant potential of 5 V for 45 minutes. Electro-polymerization was done using a standard three-electrode configuration consisting of a platinum plate (counter) electrode, a silver wire (reference) electrode and an indium tin oxide (ITO) (working) electrode on an electrochemical workstation (CHI 660D). Overnight drying in a 37 °C vacuum oven was done after extensive post-polymerization washing to eliminate excess ionic liquid and unreacted monomers. Polymer films using different ionic liquids such as $BMIMMeSO_4$ were prepared for optimization studies.

Preparation of polymer dots (Pdots)

The dried pTh polymer film was gently scraped off the ITO electrode and suspended in THF (tetrahydrofuran, Sigma Aldrich) solvent at 1 mg ml^{-1} concentration, followed by exfoliation using ultrasonication (Branson 2510; 1.1 A, 230 W) at 27 °C for 1 h. The suspension formed was then filtered using a WHATMAN 0.2 μm PTFE filter to obtain a clear yellow

[a] *School of Chemical and Biomedical Engineering, Nanyang Technological University, 70 Nanyang Drive, 637457, Singapore. E-mail: ChenPeng@ntu.edu.sg*
[b] *Institute of Materials Research and Engineering, the Agency for Science, Technology and Research (A*STAR), 2 Fusionopolis Way, #08-03, Innovis, 138634, Singapore*

† Electronic supplementary information (ESI) available: Characterization, cell imaging and antibacterial studies. See DOI: 10.1039/c6qm00065g

solution. Eventually, the THF was extracted using a rotary evaporator (Heidolf) at 30 °C.

The dried aggregates were subsequently re-suspended in DMF (*N*,*N*-dimethylformide, Sigma Aldrich) or distilled water following which the polythiophene-based Pdot (pTh-Pdots) suspensions were further purified. pTh-Pdots in DMF (green pTh-Pdots) were purified by syringe filtration through a 0.1 μm PTFE filter. On the other hand, the pTh-Pdots in water (blue pTh-Pdots) were ultra-filtered (molecular cut-off weight of 3 kDa) followed by filtration through a 0.1 μm nitrocellulose membrane to remove the aggregates. Both the green pTh-Pdots and blue pTh-Pdots were highly stable (lasting for months without apparent aggregation). Furthermore, aprotic solvents such as THF appeared to be suitable for high yield exfoliations in contrast to other solvents like ethanol and water which showed little to no exfoliation (data not shown).

Characterization

The samples were imaged using a field emission scanning electron microscope (FESEM, JMS-6700F), an atomic force microscope (MFP-3D AFM microscope, Asylum research), and a high-resolution transmission electron microscope (HRTEM, JEOL JEM 2100F TEM). Fourier transform infrared spectroscopy and X-ray photoelectron spectroscopy were performed using a Perkin Elmer FTIR Spectrometer (GX 69233), and a Kratos Axis Ultra^{DLD} spectrometer (Kratos Analytical Ltd; equipped with a monochromatized Al Kα X-ray source), respectively. The UV-Vis absorption and photoluminescence spectra were obtained using a UV-2450 spectrophotometer (Shimadzu) and an LS-55 fluorescence spectrometer (PerkinElmer), respectively.

Cell imaging

The HeLa cells (human epithelial carcinoma cell line; American Type Culture Collection) were cultured in DMEM (Life Technologies) supplemented with 10% fetal bovine serum and 1% penicillin–streptomycin, at 37 °C in a humidified atmosphere containing 5% CO_2 and 95% air. Before confocal imaging, the cells were incubated for 1–3 h with pTh-Pdots originally stocked in DMF (5 μg ml^{-1}), pTh-Pdots originally stocked in water (50 μg ml^{-1}), or LysoTracker Red DND-99 (100 nM; Life Technologies). In some experiments, the cells were transfected with mRFP-Rab5 (Addgene) using Lipofectamine3000 (Life Technologies), 1–2 days before incubation with pTh-Pdots. Confocal images were taken using a LSM710 confocal laser-scanning microscope (Carl Zeiss, Germany) upon excitation at 405 nm, 488 nm, or 580 nm.

Antibacterial studies

All bacterial strains were from the American Type Culture Collection. Optical density at 600 nm (OD 600) of the bacterial suspensions was measured using a spectrophotometer (SpectraMax M5; Molecular Devices). pTh-Pdots or/and H_2O_2 (Sigma Aldrich) were added to 2 ml of bacterial suspensions in Luria Broth (LB) solution (0.01 OD 600 corresponding to 1 × 10^6 cells per ml), to attain a final concentration of 0–100 μg ml^{-1} and 0–0.75 mM, respectively. This was followed by incubation at 37 °C for 8 or 18 h, with ~200 rpm constant shaking. The OD change after the incubation was used to assess the inhibitory effect of pTh-Pdots or antibiotics on bacterial growth. The bactericidal activity of pTh-Pdots was examined using a fluorescence viability kit (Live/Dead BacLight bacterial viability kit, Life Technologies) and FESEM. Before these imaging experiments, overnight grown *E. coli* cultures (OD 600 = 1.0, corresponding to 1 × 10^9 cells per ml) were centrifuged at 6000 rpm, followed by suspension in HBSS (Hank's balanced salt solution, Life Technologies) and 2 h incubation with or without 100 μg ml^{-1} pTh-Pdots. Subsequently, the suspension was centrifuged at 6000 rpm, washed thrice with PBS, and re-suspended in PBS. For FESEM, sample preparation follows the previously reported protocol.[11] In brief, the bacteria were fixed by 2.5% glutaraldehyde (primary fixative) in 0.1 M phosphate buffer (PB) for 1 h. The cells were then washed 3 times with PB, followed by incubation in 1% osmium tetroxide (secondary fixative) for 1 h. After washing 3 times with PB, the cells were subsequently dehydrated in ethanol with increasing concentrations (25, 50, 75, 90, and 100%). Finally, the cells were re-suspended in the mixture of hexamethyldisilazane and ethanol (1 : 1) for 15 min, followed by centrifugation at 2000 × *g*. The pellet was collected and allowed to dry overnight at room temperature.

Results and discussion

Synthesis and characterizations

As schematically illustrated in Scheme 1, polythiophene (pTh) is firstly electropolymerized from 2,2′-bithiophene (BTh) monomers in ionic liquid $BMIMBF_4$, forming a thin film on the electrode surface. $BMIMBF_4$ was used because of its wide electrochemical working window, excellent ionic conductivity and low volatility.[12] As observed by field-effect scanning electron microscopy (FESEM), the pTh film consists of micro-granules whose size increases with polymerization time (Fig. S1 in ESI†). Subsequently, pTh-Pdots are readily exfoliated from the pTh film by ultrasonication in anhydrous tetrahydrofuran (THF), yielding a yellowish homogenous suspension. Afterwards THF is completely extracted using rotary evaporation and the dried pTh-Pdots are re-suspended in dimethylformamide (DMF) or deionized water.

High-resolution transmission electron microscopy (HRTEM) reveals that the average diameter of pTh-Pdots is 2.37 ± 0.47 nm (n = 200) (Fig. 1a and b). Atomic force microscopy (AFM) shows that the average thickness of pTh-Pdots is 3.83 nm ± 0.73 nm

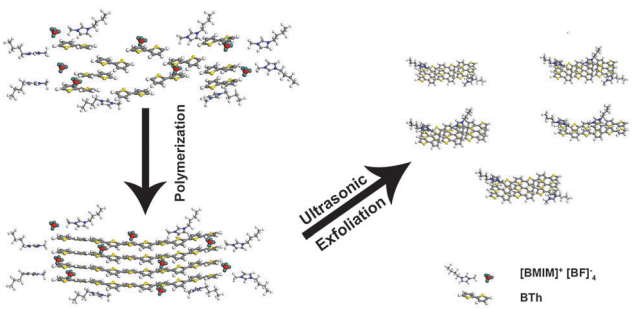

Scheme 1 Schematic illustration of pTh-Pdot synthesis.

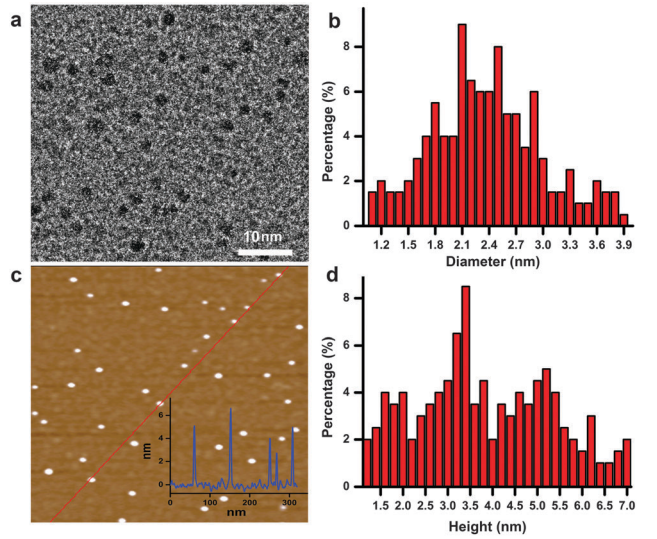

Fig. 1 (a) High-resolution TEM image of pTh-Pdots. (b) Diameter distribution (n = 200). (c) AFM image of pTh-Pdots. Inset shows the height profile along the indicated line. (d) Height distribution (n = 200).

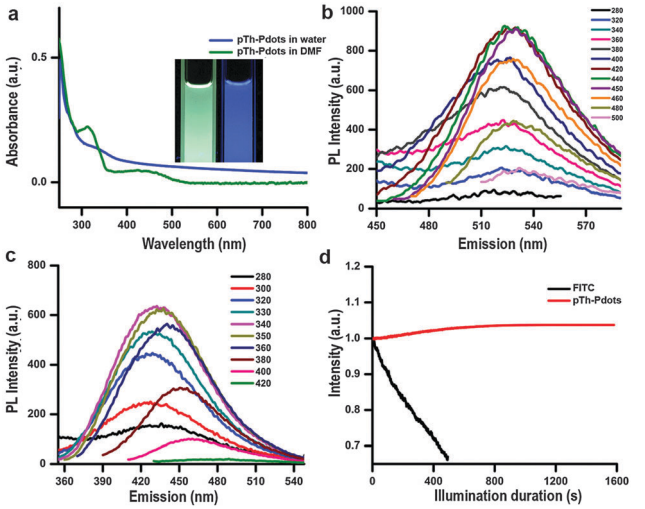

Fig. 2 (a) UV-Vis spectra of pTh-Pdots in DMF and pTh-Pdots in water. Inset shows the optical images under UV illumination at 365 nm. (b) PL emission spectra of pTh-Pdots in DMF at different excitation wavelengths. (c) PL emission spectra of pTh-Pdots in water, (d) photo-bleaching of FITC dye molecules and pTh-Pdots under confocal imaging.

(n = 200), corresponding to ~3 layers of pTh (Fig. 1c and d).[13,14] The Fourier transform infrared spectra (FTIR) of pTh-Pdots exhibit the stretching peaks for the thiophene ring (1385 cm^{-1}), C–H (1124 cm^{-1}), C–O (1084 cm^{-1}) and C–S (697 cm^{-1}), which are characteristic of pTh (Fig. S2a in ESI†).[15,16] The triplet peaks of C–H asymmetric and symmetric vibration (at 2962, 2921, and 2852 cm^{-1}) originate from the alkyl groups of $BMIM^+$ molecules adsorbed onto Pdots.[17,18] Also characteristic of pTh, X-ray photoelectron spectroscopy (XPS) shows that the high-resolution C 1s spectrum can be deconvoluted into sp^2(C═C), sp^3(C–C), C–S peaks; and the high-resolution S 2p spectrum can be split into S $2p_{3/2}$ and S $2p_{1/2}$ peaks (Fig. S2b and c in ESI†).[19,20] The N–C and N═C peaks in the high-resolution N 1s spectrum originate from the imidazole moiety of $BMIM^+$ (Fig. S2d in ESI†).[21,22] Presumably, $BMIM^+$ facilitates the exfoliation and dispersion of Pdots through pi–pi interaction with pTh.[23] We found that compared to other ionic liquids such as 1-butyl-3-methylimidazolium methyl sulphate ($BMIMMeSO_4$) and tetra ethyl ammonium chloride (TEAC), $BMIMBF_4$ offers the highest yield of pTh-Pdots.

Due to its amphiphilic properties, $BMIM^+$ assists pTh-Pdots to disperse well in both water and organic solvents (no obvious aggregation for months) (Fig. S3, ESI,† inset).[23,24] Interestingly, pTh-Pdots in DMF appear to be green while they fluoresce blue in water under 365 nm UV illumination (Fig. 2a, inset). It suggests that pTh-Pdots have negative solvatochromism, *i.e.*, a blue shift in PL emission with increasing solvent polarity. Both pTh-Pdot suspensions can efficiently absorb UV light (Fig. 2a). The excitation spectra for both suspensions exhibit two peaks resulting from π to π* and σ to π* transitions (Fig. S3 in ESI†).[25] The maximum emission peaks for green pTh-Pdots in DMF and blue pTh-Pdots in water are achieved at ~530 nm (excited by 440 nm) and ~435 nm (excited by 340 nm), respectively (Fig. 2b and c). In comparison, the 2,2′-bithiophene monomer at the concentration (dissolved in DMF; not soluble in water) does not exhibit any apparent light absorption or PL emission. PL quantum yields (QY) for the green pTh-Pdots in DMF and blue pTh-Pdots in water are calculated to be 44% (using R6G as reference) and 10% (using quinine sulfate as reference) respectively.

Negative solvatochromism of pTh-Pdots is presumably due to intra-molecular conformational changes in the conjugated backbone in the solvents of different polarities.[26] As shown in Fig. S4 (ESI†), with increasing solvent polarity (DMF, propanol, ethylene glycol, water) the emission of pTh-Pdots is blue-shifted. Based on the observation that approximately the emission peak linearly scales with the relative polarity of the solvent, our pTh-Pdot may be used as a sensor to report solvent polarity. Consistently, adding 90% water to pTh-Pdot suspension in DMF changes its color from green to blue while with the addition of 50% water the pTh-Pdots can show both blue (excited at 340 nm) and green (excited at 440 nm) emission (Fig. S5 in ESI†).

The use of organic fluorophores (*e.g.*, FITC) for bioimaging is often plagued by their poor photo-stability, *i.e.*, their fluorescence is quickly bleached under confocal laser illumination (Fig. 2d). In contrast, no obvious photo-bleaching of pTh-Pdots is observed under confocal imaging. Photobleaching of organic fluorophores is due to cleavage of covalent bonds or reactions with surrounding molecules or radicals. The high photo-stability of pTh-Pdots suggests that they are highly photochemically stable. Moreover, even at concentrations (*e.g.*, 100 μg ml^{-1}) much higher than needed for bioimaging (typically a few μg ml^{-1}), pTh-Pdots do not exert apparent cytotoxic effects on animal cells (Fig. S6 in ESI†). Taken together, the high brightness, excellent photostability, good biocompatibility, and small size of pTh-Pdots are desirable properties for bioimaging.

pTh-Pdots for cellular imaging

As a proof-of-concept demonstration, we herein use pTh-Pdots for cellular imaging of HeLa cells. Although green pTh-Pdots

stocked in DMF turn into blue after being diluted into bulk aqueous medium (Fig. S5 in ESI†), they, as compared with blue pTh-Pdots stocked in water, can be more easily uptaken by the cells (compare Fig. 3 and Fig. S7 in the ESI†). This is likely because the residual DMF molecules attached on pTh-Pdots facilitate the cell uptake.[27] Therefore, in the following bio-imaging experiments, we used pTh-Pdots originally stocked in DMF (*i.e.*, DMF decorated pTh-Pdots). As shown in Fig. 3, after 1 h incubation with pTh-Pdots (5 μg ml^{-1}), pTh-Pdots are well taken up into the cells and appear blue. Apparently, these pTh-Pdots are segregated in the early endosomes after being endocytosed because they are largely co-localized with the early endosome marker mRFP-Rab5. Interestingly, after 3 h incubation, in addition to blue pTh-Pdots in early endosomes, green pTh-Pdots also appear inside the cells. Evidently, these green pTh-Pdots stain lysosomes (but not early endosomes) because they are essentially co-localized with the lysosome marker LysoTracker Red (Fig. 3). These experiments demonstrate that pTh-Pdots can be employed to specifically label two distinct compartments (early endosomes and lysosomes) residing in the early and late endocytic pathways, respectively. As shown in Fig. S8 (ESI†), after 6 h most of the pTh-Pdots move towards lysosomes and after 24 h all of them reach lysosomes. Taken together, pTh-Pdots migrate from early endosomes to lysosomes over time.

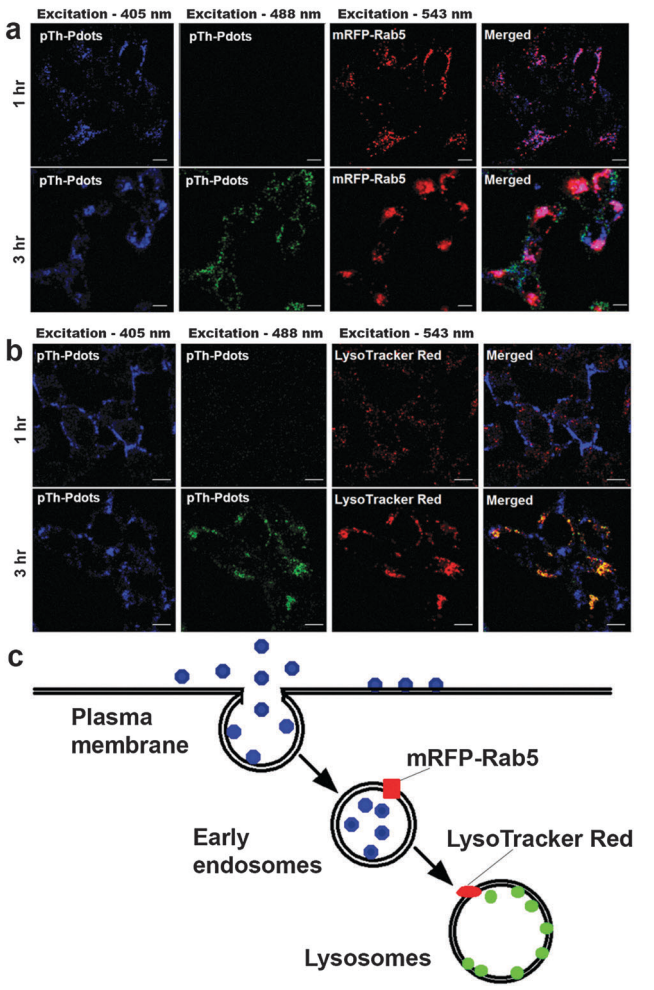

Fig. 3 Confocal imaging of HeLa cells incubated with pTh-Pdots (DMF stock diluted in cell medium to 5 μg ml^{-1}) for 1 and 3 h, respectively. (a) Co-localization with the early endosome marker (mRFP-Rab5). (b) Co-localization with the lysosome marker (LysoTracker red). (c) Schematic for the endocytosis uptake of pTh-Pdots.

We conceive that owing to their polarity-sensitive PL properties pTh-Pdots fluoresce blue in the aqueous endosome lumen whereas they turn into green in lysosome because of being inserted into a hydrophobic lysosomal membrane. As discussed earlier, although polythiophene (pTh) is highly hydrophobic, pTh-Pdots can well-disperse in aqueous solution because of the attached BMIM$^+$ moieties. It is possible that BMIM$^+$ moieties are removed or destroyed while going through the early endocytic pathway or inside lysosomes, which are highly degradative because of the presence of various enzymes. As a consequence, the hydrophobic pTh-Pdots preferably intercalate into the lysosomal membrane. To directly support this hypothesis, we show that green pTh-Pdots originally stocked in DMF turn blue on being added to bulk water (Fig. S5 in ESI†) whereas pTh-Pdots encapsulated by the amphiphilic polymer Pluronic F-127 retain green fluorescence in water (Fig. S9 in ESI†). This confirms that pTh-Pdots are green fluorescent in a hydrophobic environment. We further show that pTh-Pdots incorporated into the lipid bilayers of artificial liposomes are green (Fig. S9 in ESI†).

pTh-Pdots as antibacterial agents

With certain thiophene derivatives being known as good antibacterial agents,[28,29] we speculate that pTh-Pdots can be used as antibacterial agents. Indeed, it is found that pTh-Pdots are very effective against both Gram-negative [G(−); *E. coli* and *P. aeruginosa*] and Gram-positive [G(+); *S. aureus*] bacteria, with low minimum inhibitory concentrations (MIC, lowest concentration to cause appreciable inhibition of bacterial growth). For these bacterial strains, the potency of pTh-Pdots is comparable to a commonly used broad-spectrum antibiotic (kanamycin). Dose dependent studies show that pTh-Pdots are most effective against *E. coli* with MIC ~45 μg ml^{-1}, followed by *S. aureus* (MIC ~ 60 μg ml^{-1}) and *P. aeruginosa* (MIC ~ 100 μg ml^{-1}) (Fig. 4a and b and Fig. S10 in ESI†). Unsurprisingly, pTh-Pdots are more potent to G(−) bacteria than G(+) bacteria which are protected by a thick peptidoglycan surface layer.

Some pathogenic *E. coli* strains can be life threatening and resistant to antibiotics. As shown in Fig. 4c, pTh-Pdots can efficiently kill ampicillin-resistant *E. coli*. On the other hand, pTh-Pdots are highly biocompatible to mammalian cells (primary rat fibroblast cells in Fig. 4d; HeLa cells in Fig. S6 in ESI†). The antibacterial capability of pTh-Pdots does not originate from BMIM$^+$ moieties attached on their surface because $BMIMBF_4$ ionic liquid even at a high concentration of 0.5 mg ml^{-1} is incapable of causing bacterial death (Fig. S11 in ESI†).

Also interestingly, we discover that the pTh-Pdot is an excellent peroxidase mimic, which converts H_2O_2 into hydroxyl radicals ($^{\bullet}OH$) (Fig. S12 in ESI†). Graphene quantum dots (GQDs) have also been found to show peroxidase activities.[30,31]

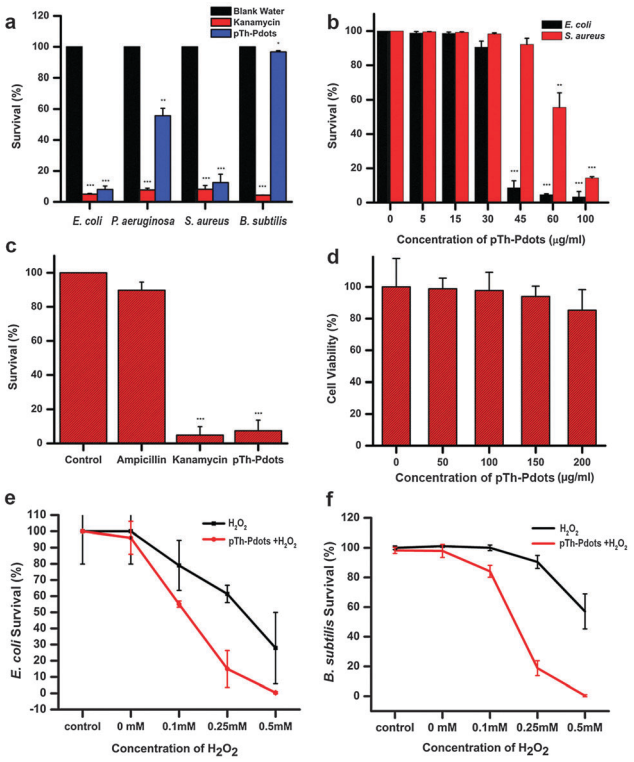

Fig. 4 Antibacterial activity of pTh-Pdots. (a) Viability test against G(+) and G(−) bacteria with 100 μg ml^{-1} pTh-Pdots. (b) Dose dependent effect of pTh-Pdots against G(+) and G(−) bacteria. (c) Viability test of ampicillin-resistant *E. coli* treated with ampicillin, kanamycin and pTh-Pdots (all at 100 μg ml^{-1}). (d) MTT assay of rat fibroblasts after overnight incubation with pTh-Pdots at various concentrations. (e and f) Viability tests of *E. coli* (e) and *B. subtilis* (f) treated with H_2O_2 at different concentrations with or without pTh-Pdots (10 μg ml^{-1}).

Taking advantage of this, they have been used to improve the antibacterial performance of H_2O_2 for wound disinfection.[32] We found that pTh-Pdots possess much higher peroxidase activity than GQDs (Fig. S12 in ESI†). Although pTh-Pdot itself cannot kill Gram-positive *B. subtilis* (Fig. 4a), the synergistic effect between pTh-Pdots and H_2O_2 is potent (Fig. 4f). pTh-Pdots can greatly enhance the potency of H_2O_2 in killing both Gram-negative (Fig. 4e) and Gram-positive strains (Fig. 4f).

We speculate that the antimicrobial activity of the positively charged pTh-Pdots (zeta potential ζ = 21.2 mV) may be realized by disrupting the negatively charged bacterial membrane through electrostatic interaction. Indeed as shown in Fig. 5a, in the presence of a viability testing dye mixture (SYTO 9/propidium iodide), live bacteria appear green due to SYTO 9 staining whereas dying or dead bacteria after pTh-Pdot treatment appear yellow or red due to the uptake of red propidium iodide through a compromised cell membrane. Consistently, field-effect scanning electron microscopy (FESEM) also shows that the bacterial membrane becomes crumpled after pTh-Pdot treatment (Fig. 5b).

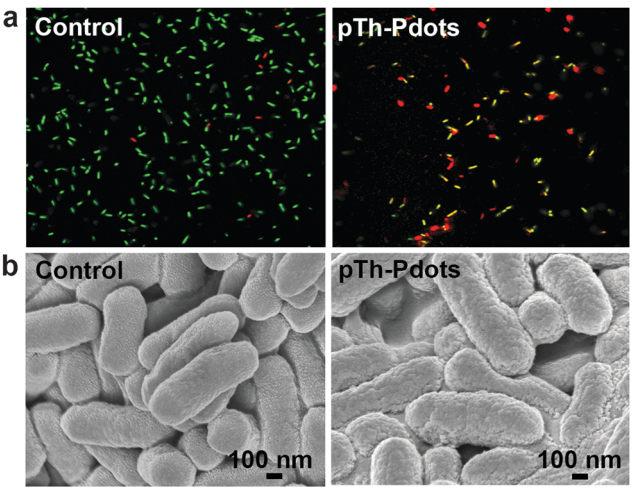

Fig. 5 Fluorescence images with live/dead dye staining (a) and FESEM images of *E. coli* cells (b) without (left column) or with (right column) incubation of pTh-Pdots (100 μg) for 2 h.

Conclusion

In summary, we have synthesized a new fluorescent polymer dot derived from non-fluorescent polythiophene (pTh-Pdots) using a simple and high yield procedure. These pTh-Pdots are bright, stable, biocompatible and small, and therefore promising for bioimaging applications. Exploiting its negative solvatochromism properties, here we demonstrate the use of pTh-Pdots in live cells to label and differentiate early endosomes and lysosomes along the endocytic pathway. We further demonstrate that, making use of their ability to disrupt the bacterial membrane and mimic peroxidase activity, pTh-Pdots can serve as potent antibacterial agents against both Gram-negative and Gram-positive bacteria, even drug-resistant strains. Different types of Pdots may be similarly synthesized simply by changing the polymeric precursors (fluorescent or non-fluorescent, conducting or semiconducting). Distinct to other reported polymer dots, which are made by condensing the long-chain fluorescent semiconducting polymers, the Pdots presented here are synthesized from the bottom up and are much smaller. Such a new class of zero-dimensional nanomaterials, which may be viewed as heteroatom-doped carbon nanoparticles and fluoresce due to quantum confinement induced bandgap opening,[33,34] shall find a wide range of novel applications.

Acknowledgements

This work was supported by the Ministry of Education of Singapore under the AcRF Tier 2 grant (MOE2014-T2-1-003), AcRF Tier 1 grant (M4011559.120, RG133/15) and the Nanyang Technological University start-up grant (NTU-SUG: M4081627.120).

Notes and references

1 C. Wu and D. T. Chiu, *Angew. Chem., Int. Ed. Engl.*, 2013, **52**, 3086–3109.
2 Z. Tian, J. Yu, C. Wu, C. Szymanski and J. McNeill, *Nanoscale*, 2010, **2**, 1999–2011.

3 R. I. Dmitriev, S. M. Borisov, H. Dussmann, S. Sun, B. J. Muller, J. Prehn, V. P. Baklaushev, I. Klimant and D. B. Papkovsky, *ACS Nano*, 2015, **9**, 5275–5288.
4 X. B. Zhou, H. Liang, P. F. Jiang, K. Y. Zhang, S. J. Liu, T. S. Yang, Q. Zhao, L. J. Yang, W. Lv, Q. Yu and W. Huang, *Adv. Sci.*, 2016, **3**, 1500155.
5 Y. R. Zhang, L. Pang, C. Ma, Q. Tu, R. Zhang, E. Saeed, A. Mahmoud and J. Y. Wang, *Anal. Chem.*, 2014, **86**, 3092–3099.
6 D. Zhang, M. Wu, Y. Y. Zeng, N. S. Liao, Z. X. Cai, G. Liu, X. L. Liu and J. F. Liu, *J. Mater. Chem. B*, 2016, **4**, 589–599.
7 J. Pecher and S. Mecking, *Chem. Rev.*, 2010, **110**, 6260–6279.
8 C. Wu, C. Szymanski, Z. Cain and J. McNeill, *J. Am. Chem. Soc.*, 2007, **129**, 12904–12905.
9 K. Landfester, R. Montenegro, U. Scherf, R. Guntner, U. Asawapirom, S. Patil, D. Neher and T. Kietzke, *Adv. Mater.*, 2002, **14**, 651–655.
10 K. P. Prasad, Y. Chen, M. A. Sk, A. Than, Y. Wang, H. D. Sun, K. H. Lim, X. C. Dong and P. Chen, *Mater. Horiz.*, 2014, **1**, 529–534.
11 E. R. Fischer, B. T. Hansen, V. Nair, F. H. Hoyt and D. W. Dorward, *Curr. Protoc. Microbiol.*, John Wiley & Sons, Inc., 2012, vol. 25, pp. 2B.2.1–2B.2.47.
12 Y. H. Pang, X. Y. Li, G. Y. Shi, F. Wang and L. T. Jin, *Thin Solid Films*, 2008, **516**, 6512–6516.
13 J. H. Liu, I. A. Mikhailov, I. Osaka, A. E. Masunov, R. D. McCullough and L. Zhai, *Polymer*, 2011, **52**, 2302–2309.
14 G. Adam, A. Pivrikas, A. M. Ramil, S. Tadesse, T. Yohannes, N. S. Sariciftci and D. A. M. Egbe, *J. Mater. Chem.*, 2011, **21**, 2594–2600.
15 B. Massoumi, N. Alipour, S. Fathalipour and M. Jaymand, *High Perform. Polym.*, 2015, **27**, 161–170.
16 D. Sun, L. Jin, Y. Chen, J. R. Zhang and J. J. Zhu, *ChemPlusChem*, 2013, **78**, 227–234.
17 A. Ananthanarayanan, X. W. Wang, P. Routh, B. Sana, S. Lim, D. H. Kim, K. H. Lim, J. Li and P. Chen, *Adv. Funct. Mater.*, 2014, **24**, 3021–3026.
18 S. Cha, M. Ao, W. Sung, B. Moon, B. Ahlstrom, P. Johansson, Y. Ouchi and D. Kim, *Phys. Chem. Chem. Phys.*, 2014, **16**, 9591–9601.
19 E. L. Ratcliff, R. C. Bakus, G. C. Welch, T. S. van der Poll, A. Garcia, S. R. Cowan, B. A. MacLeod, D. S. Ginley, G. C. Bazan and D. C. Olson, *J. Mater. Chem. C*, 2013, **1**, 6223–6234.
20 E. Z. Kurmaev, S. N. Shamin, V. R. Galakhov, A. Moewes, T. Otsuka, S. Koizume, K. Endo, H. E. Katz, M. Bach, M. Neumann, D. L. Ederer and M. Iwami, *Phys. Rev. B: Condens. Matter Mater. Phys.*, 2001, **64**, 452111.
21 H. J. Kim, I. S. Bae, S. J. Cho, J. H. Boo, B. C. Lee, J. Heo, I. Chung and B. Hong, *Nanoscale Res. Lett.*, 2012, **7**, 1–7.
22 O. Hofft, S. Bahr, M. Himmerlich, S. Krischok, J. A. Schaefer and V. Kempter, *Langmuir*, 2006, **22**, 7120–7123.
23 T. L. Greaves and C. J. Drummond, *Chem. Soc. Rev.*, 2008, **37**, 1709–1726.
24 M. L. Wang, Y. Q. Gao, J. J. Zhang and J. W. Zhao, *Electrochim. Acta*, 2015, **155**, 236–243.
25 A. Baheti, C. P. Lee, K. R. Thomas and K. C. Ho, *Phys. Chem. Chem. Phys.*, 2011, **13**, 17210–17221.
26 M. Leclerc, G. Dufresne, P. Blondin, J. Bouchard, M. Belletete and G. Durocher, *Synth. Met.*, 2001, **119**, 45–48.
27 M. Katz and B. J. Poulsen, in *Concepts in Biochemical Pharmacology: Part 1*, ed. B. B. Brodie, J. R. Gillette and H. S. Ackerman, Springer Berlin Heidelberg, Berlin, Heidelberg, 1971, vol. XXVIII, pp. 103–174.
28 R. Wilson, P. Kumar, V. Parashar, C. Vilchèze, R. Veyron-Churlet, J. S. Freundlich, S. W. Barnes, J. R. Walker, M. J. Szymonifka, E. Marchiano, S. Shenai, R. Colangeli, W. R. Jacobs Jr, M. B. Neiditch, L. Kremer and D. Alland, *Nat. Chem. Biol.*, 2013, **9**, 499–506.
29 M. L. Cerrada, A. Munoz-Bonilla and M. Fernandez-Garcia, *Polymeric Materials with Antimicrobial Activity: From Synthesis to Applications*, The Royal Society of Chemistry, 2014, pp. 387–405.
30 N. Li, A. Than, X. Wang, S. Xu, L. Sun, H. Duan, C. Xu and P. Chen, *ACS Nano*, 2016, **10**, 3622–3629.
31 H. Sun, A. Zhao, N. Gao, K. Li, J. Ren and X. Qu, *Angew. Chem.*, 2015, **54**, 7176–7180.
32 H. J. Sun, N. Gao, K. Dong, J. S. Ren and X. G. Qu, *ACS Nano*, 2014, **8**, 6202–6210.
33 X. T. Zheng, A. Ananthanarayanan, K. Q. Luo and P. Chen, *Small*, 2015, **11**, 1620–1636.
34 D. V. Lap, D. Grebner and S. Rentsch, *J. Phys. Chem. A*, 1997, **101**, 107–112.